Spiral Galaxies

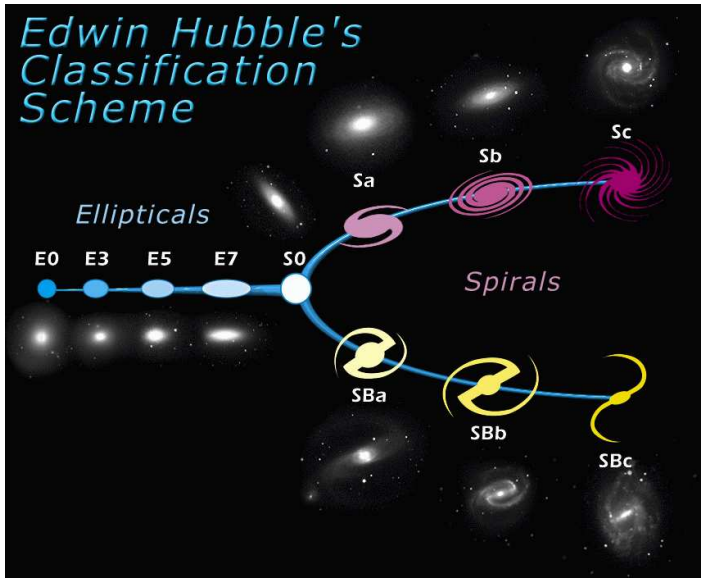

SDSS

Galaxy classification via the Hubble "tuning fork diagram":
"early types": elliptical galaxies; "late types": spiral galaxies. See homework.

Spiral Galaxies

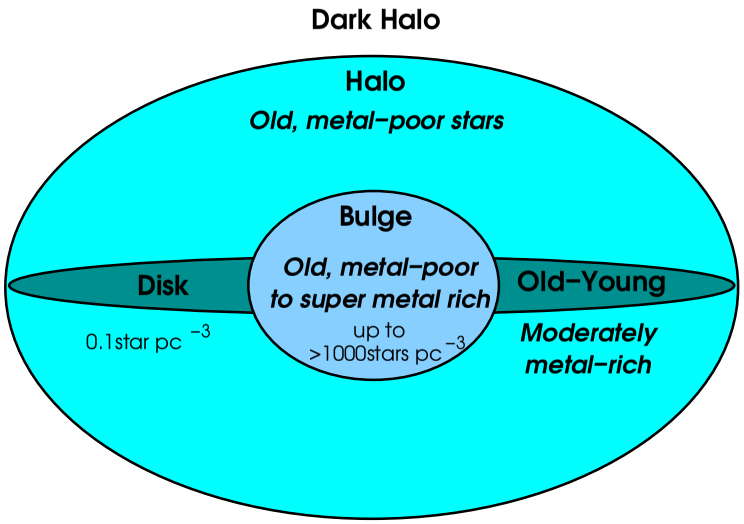

(after Prantzos, 2008; Pagel, 2009)

Spiral Galaxies

Despite many problems, it is often possible to roughly classify stars into five different populations:

Population	Typical stars	Velocity Disp. (km s^{-1})	Shape	Abundance wrt. H
Halo pop. II	globular clusters red giants	130	spherical	0.003
Intermediate pop. II	high-v stars	50	intermediate	0.01
Disk pop.		30	intermediate	0.02
Intermediate pop. I	stars with strong lines	20	intermediate	0.03
Extreme pop. I	blue supergiants	10	Flat	0.04

after Combes et al.

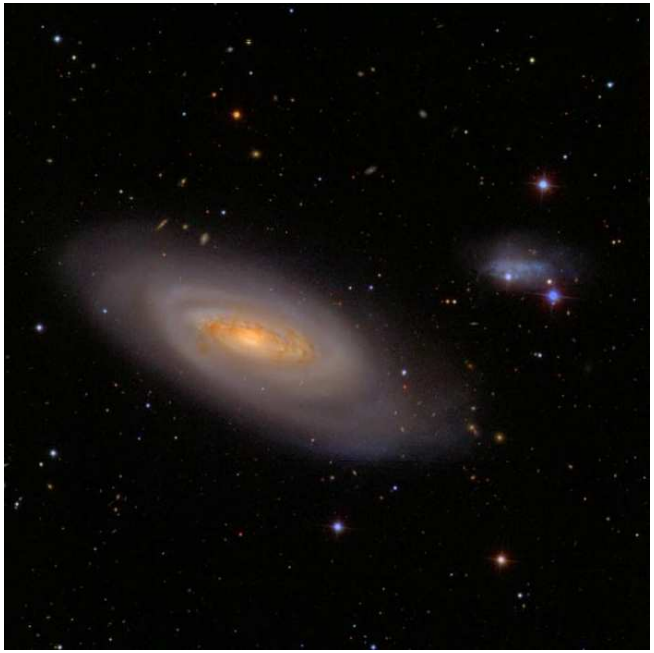

Optical light: emission from Galaxies is dominated by emission from

- stars
- emission nebulae

M90 (SDSS)

Starlight, II

4–6

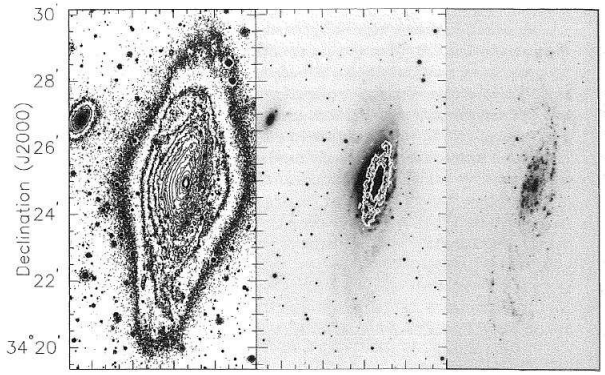

Left: R-band isophotes of NGC 7331, Middle: R-band image & CO emission, Right: Hα (SG Fig. 5.3).

There is lots of structure on galaxy images:
Bulge: circular isophotes $\Longrightarrow$ spherical distribution
Disk: isophotes elliptical $\Longrightarrow$ projection effect
inclination of NGC 7331: $\sim 75°$

Disk, I

4–7

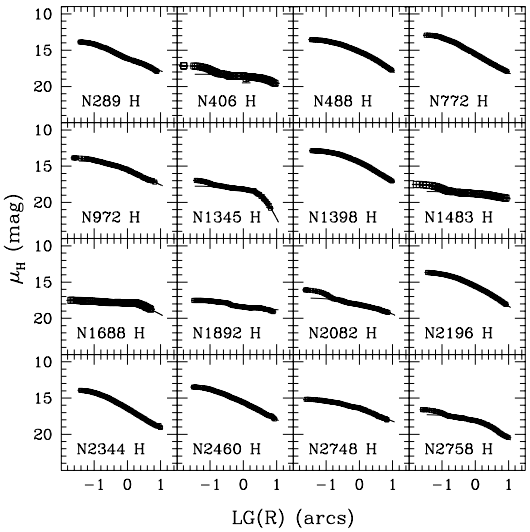

To get rid of structure: average over disk $\Longrightarrow$ surface brightness profile

(Seigar et al., 2002, Fig. 1a)

Disk, II

4–8

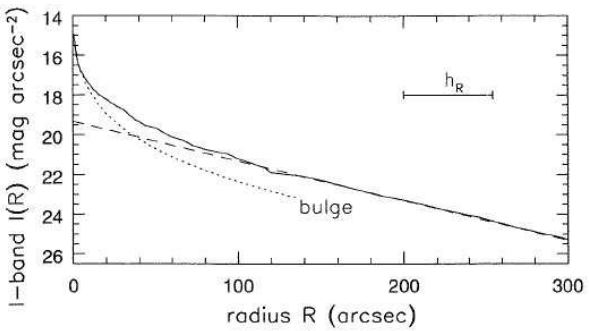

NGC7331: Surface brightness in I-band ($\sim$8000Å) (SG, Fig. 5.4);
Note: magnitudes are logarithmic: 5 mag = factor 100!

Generally surface brighness given in mag arcsec^{-2}, which is independent of distance.

For historical reasons edge of disk defined as where $I_B = 25$ mag arcsec^{-2} (R_{25}-radius)

Also sometimes used: Holmberg-radius ($I_B = 26.5$ mag arcsec^{-2})

For many spirals the disk component is well modeled by

$$I(R) = I_0 \exp(-R/h_R) \tag{4.1}$$

where scale length 1 kpc $\lesssim h_R \lesssim$ 10 kpc and where typically $I_{0,B} \sim 22$ mag arcsec^{-2}.

Note that surface brightness is higher by $1/\cos i$ when disk is tilted.

R. Gendler

Bulge: well described by de Vaucouleurs' law:

$$\log\left(\frac{I(R)}{I_e}\right) = -3.3307\left[\left(\frac{R}{R_e}\right)^{1/4} - 1\right] \tag{4.3}$$

where R_e: effective radius, i.e., radius containing in half of the total luminosity.

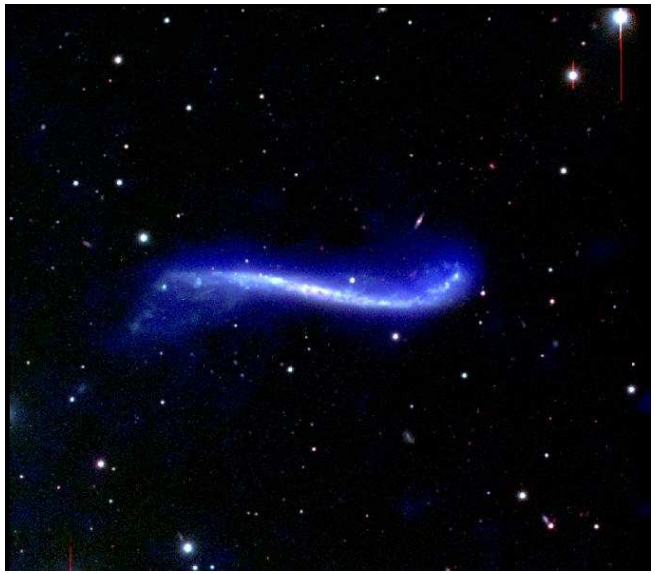

UGC 3697 ("Integral sign galaxy", a superthin galaxy; NRAO/AUI)

Vertical structure (z-direction): surface brightness well described by

$$I(R,z) = I(R)\exp\left\{-\frac{|z|}{h_z}\right\} \quad \text{where} \quad h_z \sim 0.1 h_R \tag{4.2}$$

4–12

Sequence of Disk Galaxies

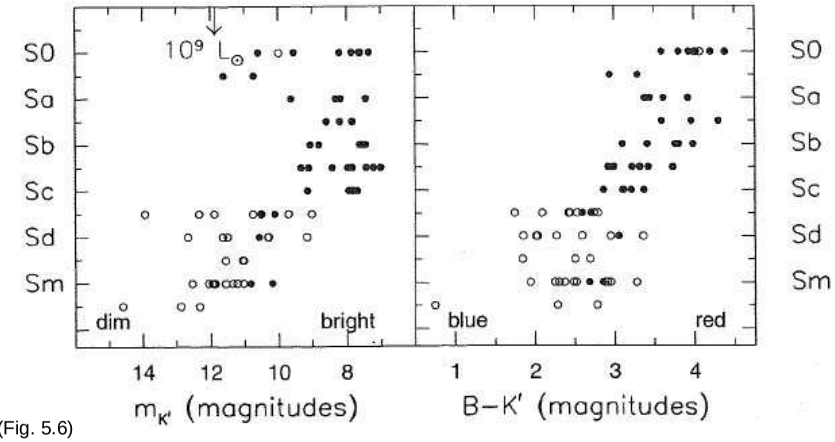

SG (Fig. 5.6)

S0 galaxies are luminous and red, while Sc and later are fainter and bluer

Sd: no bulge visible, Sm: Magellanic systems

Sequence of Disk Galaxies

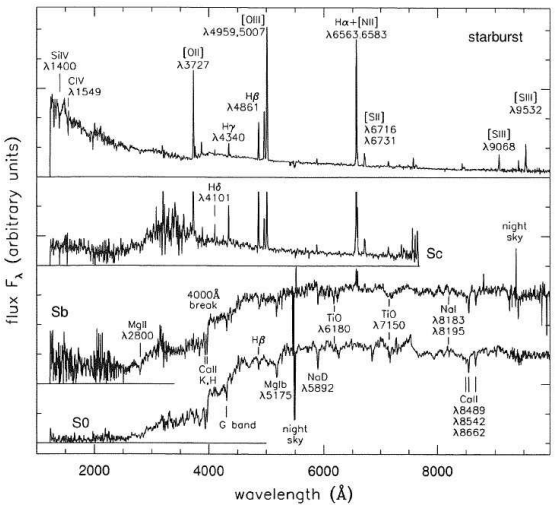

SG (Fig. 5.24)

galaxy spectra = $\sum$ constituent spectra

- S0: mainly absorption lines from cool K stars, Ca H, K from G-type stars
- Sc: mainly blue and UV emission, i.e., hot and young stars; emission lines from photoionized emission nebulae
- Starburst: significant photoionization present (see later)

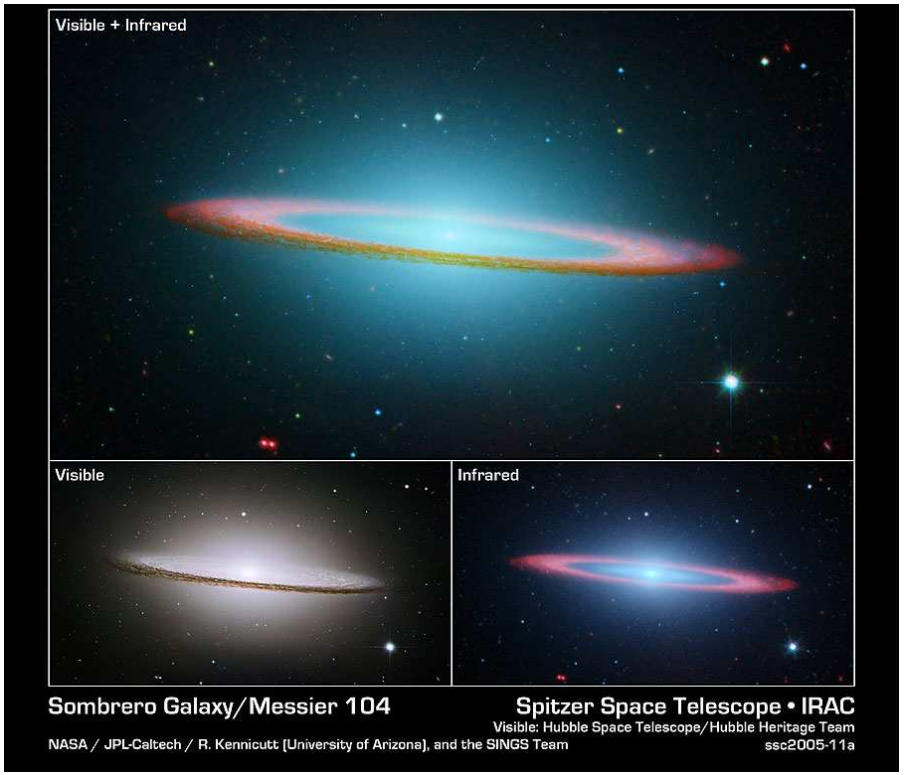

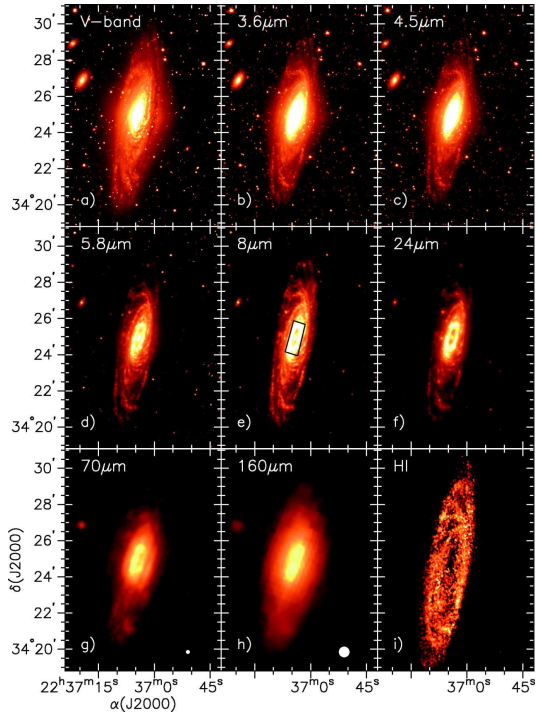

Multi-Color Image of NGC 7331, ISM mass is $5 \times 10^9\, M_\odot$.

Distribution of gas in disk mainly done using 21 cm imaging, dust using IR observations

We can generally trace H I to 10^{19} H atoms cm^{-2}, or $\sim$0.1 $M_\odot$ pc^{-2}.

(Regan et al., 2004)

Distribution of Gas and Dust

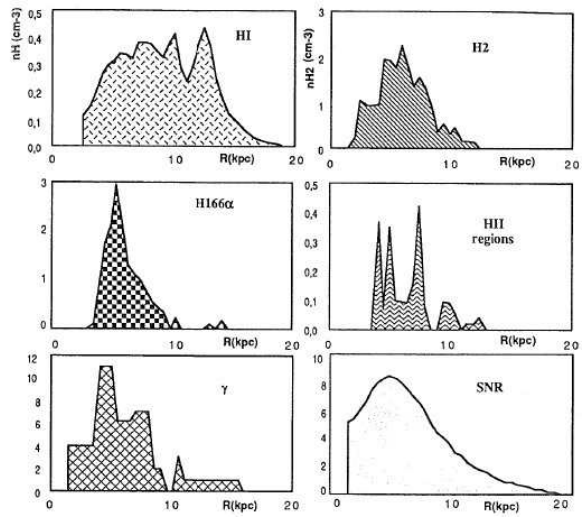

The distribution of different ISM components in Milky Way is typical for galaxies.

H166α: recombination line, traces H II regions
γ: brightness in γ-rays

Combes et al. (Fig. 2.6)

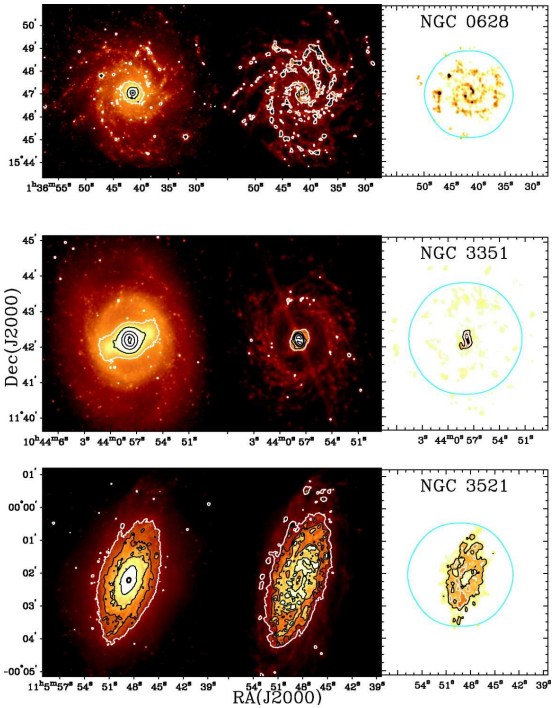

- Left: 3.6 μm: red giant stars
- Middle: 0.8 μm, stellar continuum-subtracted: PAHs
- Right: CO(1-0) mosaic (circle: outer range of detection)

(Regan et al., 2006, Fig. 1)

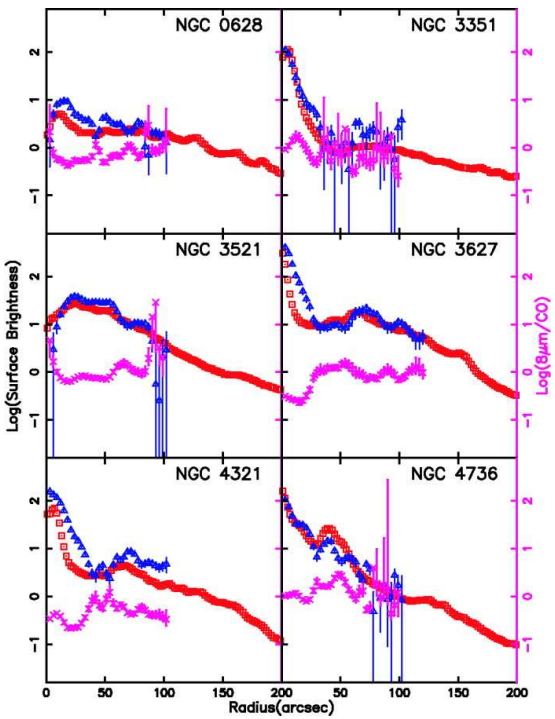

Radial intensity profiles:

- red: PAH
- blue: CO
- magenta: ratio

(Regan et al., 2006, Fig. 3)

Distribution of Gas and Dust

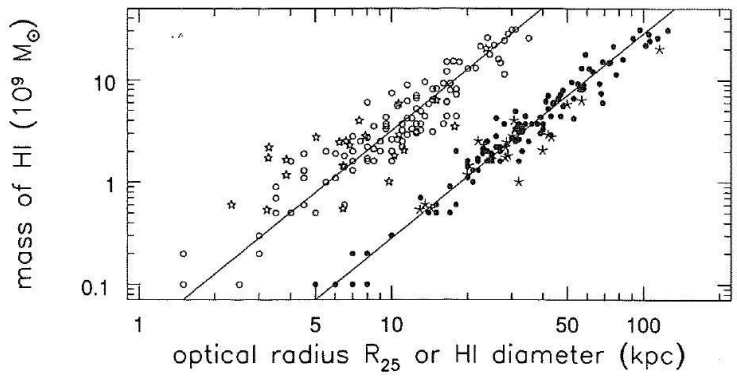

SG (Fig. 5.15)

Mass of H I gas as function of

- the optical radius R_{25} (open circles; note: $\propto R_{25}^2$; slope: 10 $M_\odot$ pc^{-2})
- the diameter where surface density drops to 1 $M_\odot$ pc^{-2} (filled circles; slope: 3.6 $M_\odot$ pc^{-2} within diameter)

$\Longrightarrow$ H I disk extends generally to $\sim 2R_{25}$

Distribution of Gas and Dust

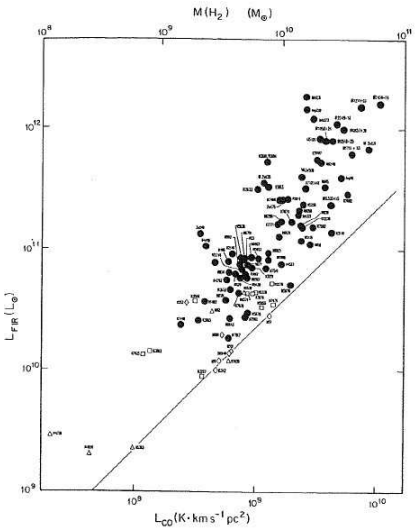

The IR luminosity and the CO luminosity (=H_2-content) of spirals are generally correlated.

Line: milky way

$L_{\rm IR}/M_{\rm H_2}$: good indicator for star formation, for normal spirals ratio is 1…3, for starbursts 20–30, for "IRAS-galaxies" can reach 200.

Combes et al. (Fig. 2.11)

Radio Emission, I

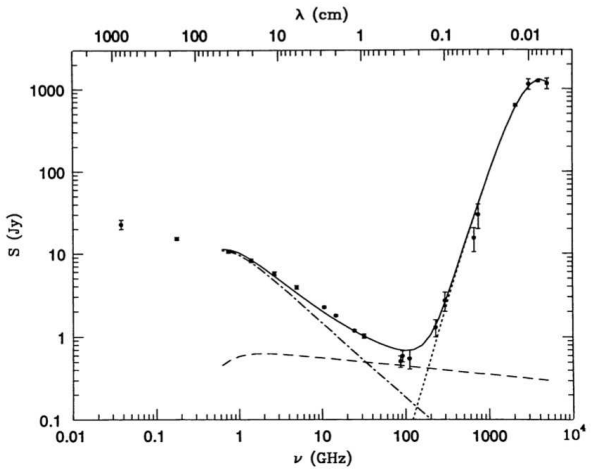

Condon (1992)

- thermal emission (dust; high frequencies)
- free-free Bremsstrahlung (ionized medium; intermediate frequencies)
- a power-law component at low frequencies.

Next: What does the power-law component look like in radio images?

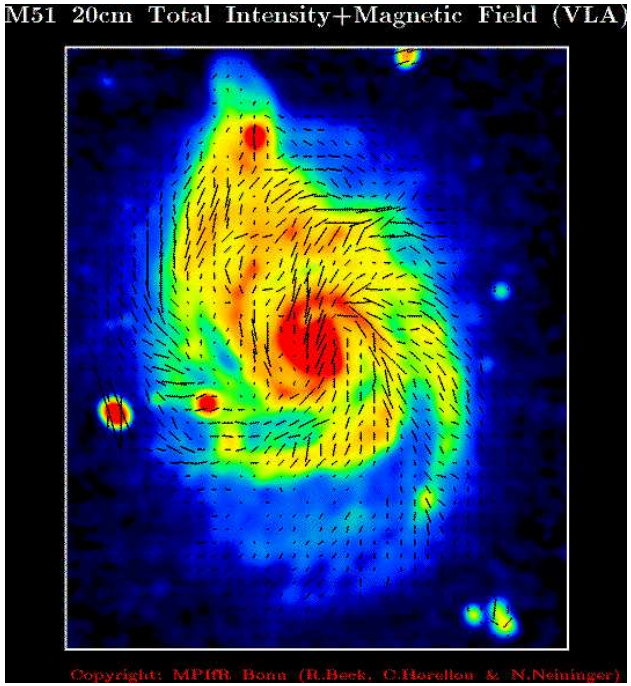

Non-thermal radio emission traces spiral arms and is strongly polarized

Next: What process can produce this kind of emission?

Synchrotron Emission, I

Magnetic fields: trace through synchrotron radiation from electrons moving around B-field lines.

Lorentz-force (Gaussian units!):

$$\frac{d\boldsymbol{p}}{dt} = \frac{e}{c}\boldsymbol{v} \times \boldsymbol{B} \quad \text{where} \quad \boldsymbol{p} = \frac{m_\mathrm{e}\boldsymbol{v}}{\sqrt{1-\beta^2}} = \gamma m_\mathrm{e}\boldsymbol{v} \quad \text{with} \quad \gamma = \frac{1}{\sqrt{1-\beta^2}} \quad \text{and} \quad \beta = \frac{v}{c} \tag{4.4}$$

Therefore the acceleration is

$$\frac{d\boldsymbol{v}}{dt} = \frac{e}{c\gamma m_\mathrm{e}}\boldsymbol{v} \times \boldsymbol{B} \tag{4.5}$$

Since $\boldsymbol{v} \times \boldsymbol{B}$ is always perpendicular to $\boldsymbol{v}$ and $\boldsymbol{B}$, the component of $\boldsymbol{v}$ along the B-field does not change. This constant perpendicular force results to a helical motion around the B-field line with the frequency

$$\omega_B = \frac{eB}{\gamma m_\mathrm{e} c} = \frac{\omega_\mathrm{L}}{\gamma} \quad \text{with the Larmor frequency} \quad \omega_\mathrm{L} = 2\pi\nu_\mathrm{L} = \frac{eB}{m_\mathrm{e}c} \tag{4.6}$$

For typical ISM values, the Larmor frequency and Larmor radius are

$$\nu_\mathrm{L} = 2.8 \times 10^6 B_{10^{-6}\,\mathrm{G}}\,\mathrm{MHz} \quad \text{and} \quad R_\mathrm{L} = \frac{\gamma v_\perp}{\omega_\mathrm{L}} \sim 2\,\mathrm{AU} \cdot \frac{E}{1\,\mathrm{GeV}} \cdot \left(\frac{B}{10^{-6}\,\mathrm{G}}\right)^{-1} \tag{4.7}$$

Synchrotron Emission, II

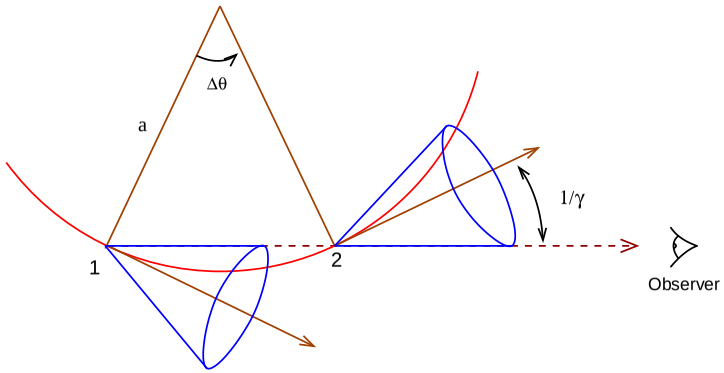

(after Fig. 6.2 of Rybicki & Lightman, 1979)

Electrons are accelerated, and therefore radiate. For relativistic electrons: radiation is forward beamed into cone with opening angle $\Delta\theta \sim 1/\gamma$. In the Electron frame of rest: beam passes observer during time

$$\Delta t = \frac{\Delta\theta}{\omega_B} = \frac{m_\mathrm{e}c\gamma}{eB}\frac{2}{\gamma} = \frac{2}{\omega_\mathrm{L}} \tag{4.8}$$

Synchrotron Emission, III

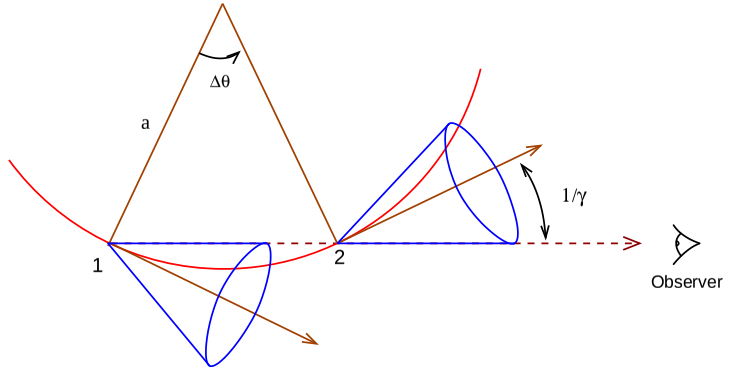

(after Fig. 6.2 of Rybicki & Lightman, 1979)

Observer frame: Doppler effect! (electron is closer to us at end of time interval)

$\Longrightarrow$ observed pulse duration:

$$\tau = \left(1 - \frac{v}{c}\right) \Delta t = (1 - \beta)\Delta t \qquad (4.9)$$

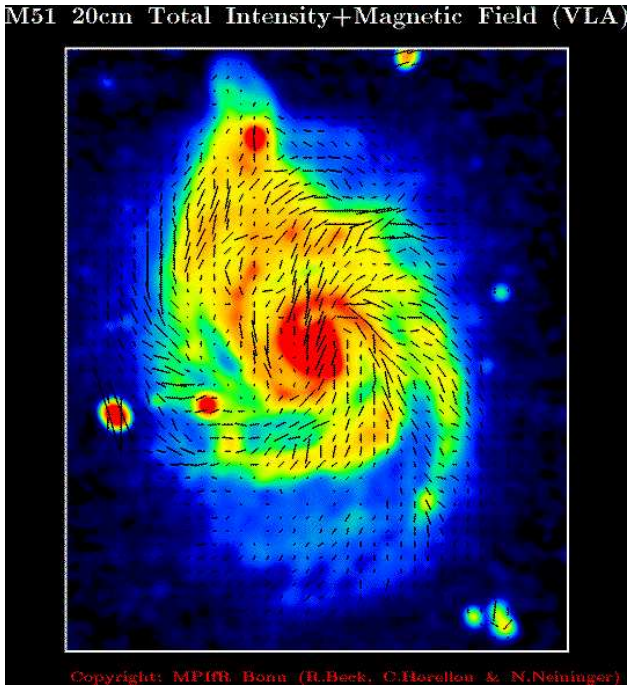

In addition to spectral shape, synchrotron radiation is strongly polarized.
Polarization can be used to find B-field vectors!

B-field vectors inferred from the degree of polarization in spiral galaxy M51 by rotation of the observed E-field-vectors by 90°

(Neininger 1992, A&A 263, 30)

Synchrotron Emission, IV

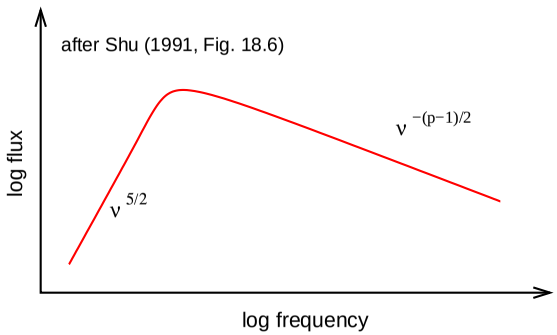

At low ν: synchrotron emitting electrons can absorb synchrotron photons:
synchrotron self-absorption.

For a power law electron distribution $\propto E^{-p}$, total spectral shape can be shown to be:

For low frequencies: $P_\nu \propto B^{-1/2}\nu^{5/2}$ (independent of p!)
For large frequencies: $P_\nu \propto \nu^{-(p-1)/2}$

One often uses the terms optically thick/thin to describe the absorbed/unabsorbed part of a synchrotron spectrum. The turnover describes the $\tau = 1$ surface, e.g., of a jet. In general: $\tau \propto R$ (R: size of the emitting region). More compact regions are optically thick, more extended regions are optically thin.

Spider Diagrams, I

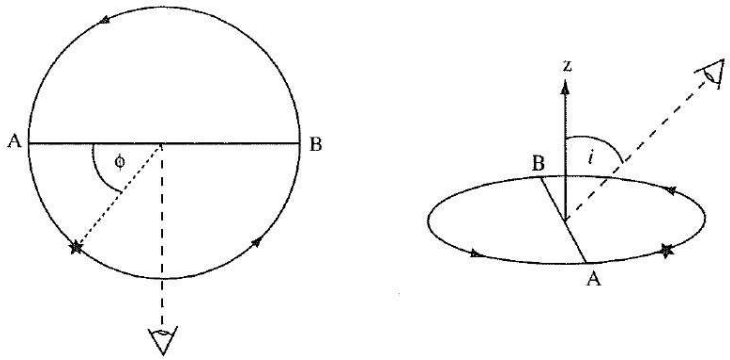

Now consider motion of gas in spiral galaxies.

Good assumption for now: gas is moving on approximately circular orbits

Spider Diagrams, II

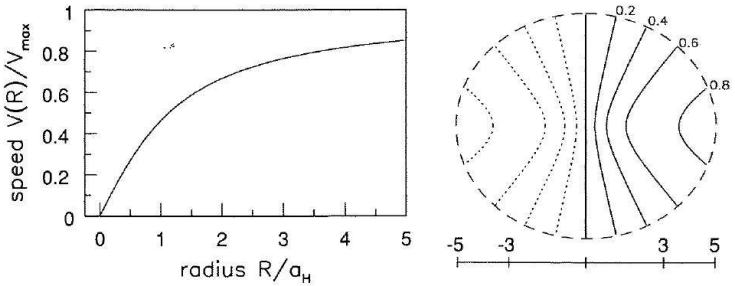

Because we look at inclined galaxy, observed radial velocity is given by

$$v_r(R,i) = v_{\text{syst}} + v(R)\sin i\cos\phi \qquad (4.10)$$

where v_{syst} is the systemic velocity (e.g., peculiar velocity plus Hubble flow), and where $v(R)$ is the rotational velocity.

Observations: plot curves of constant v_r: Spider diagram

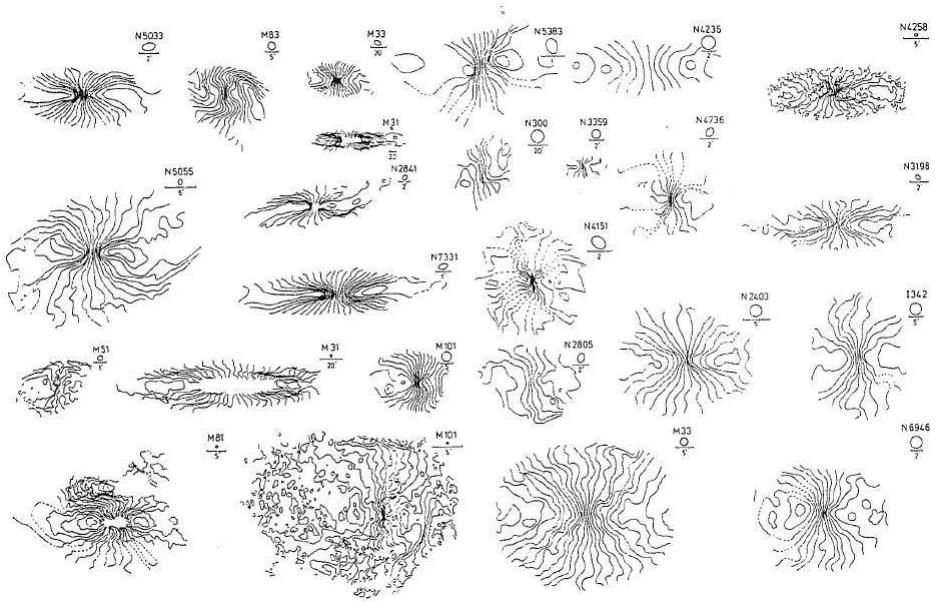

Combes et al. (Fig. 3.5)

Spider Diagrams, IV

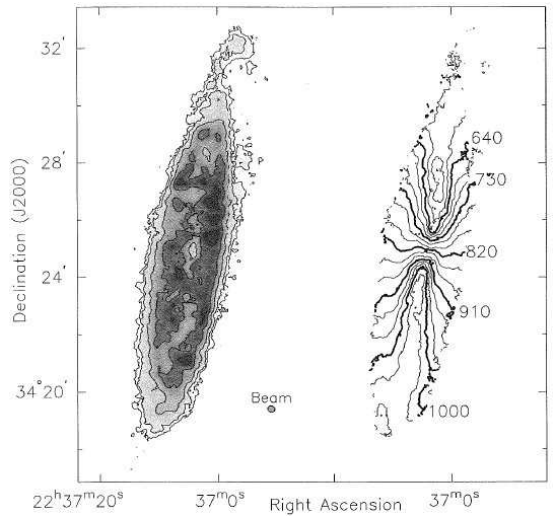

Major properties of spider diagrams:

- central regions: contours parallel to minor axis $\Longrightarrow V(R) \propto R$
- outer regions: contours radial $\Longrightarrow V(R) \sim$ const.

H I gas surface density and gas velocity in NGC 7331 (SG, Fig. 5.13)

Rotation Curves, I

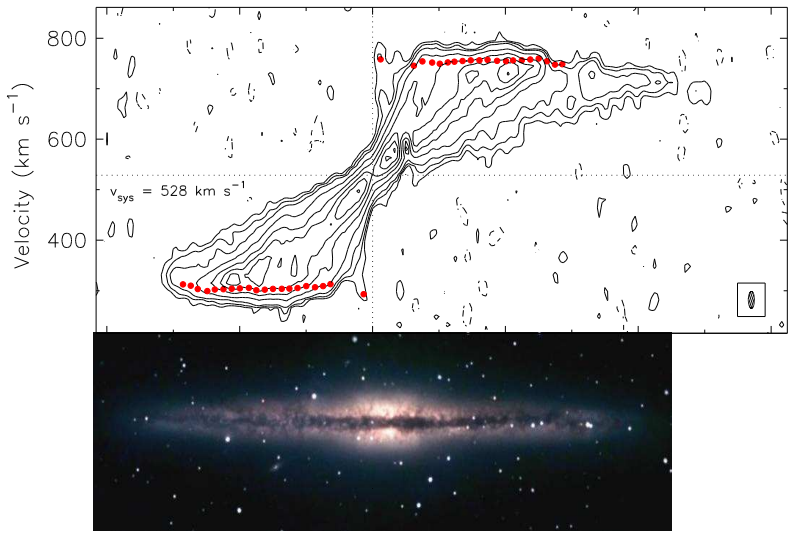

NGC 891 (Swaters et al., 1997, ApJ 491, 140 / Paul LeFevre, S&T Nov. 2002)

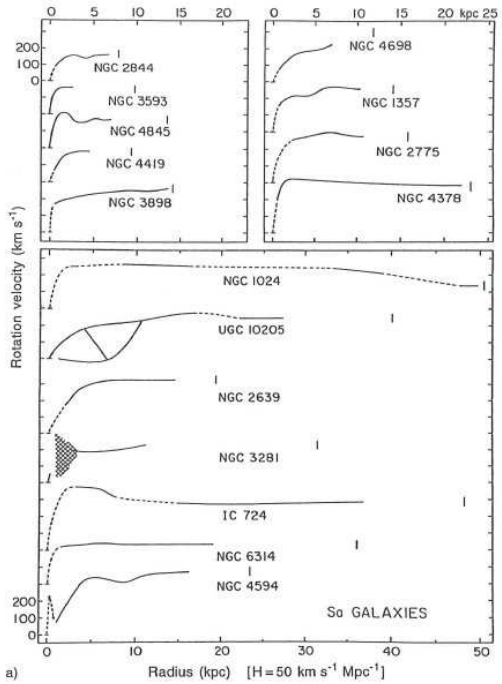

Rotation curves of Sa galaxies (Combes et al., Fig. 3.1)

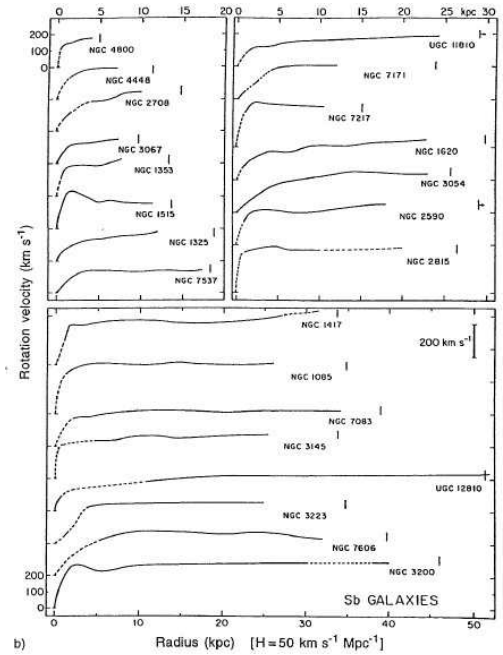

Rotation curves of Sb galaxies (Combes et al., Fig. 3.1)

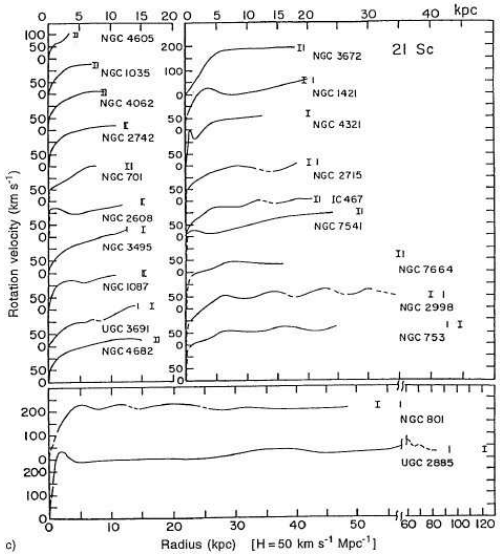

Rotation curves of Sc galaxies (Combes et al., Fig. 3.1)

Rotation Curves, V

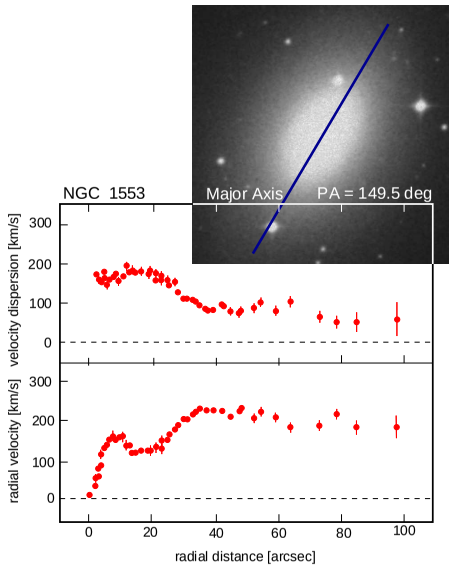

Spiral galaxy rotation curves are flat!

"Galaxy rotation problem", first discovered by Vera Rubin (1970)

©Astron. Soc. Pacific

← NGC 1553 (S0) (after Kormendy, 1984, ApJ 286, 116)

Rotation Curves, VI

To derive gas motion: assume that gas is in dynamic equilibrium and that the motion is solely determined by gravity.

The equation of motion

$$\ddot{\boldsymbol{r}} = -\nabla\Phi \tag{4.11}$$

where the potential is obtained from solving Poisson's equation

$$\Delta\Phi(R) = 4\pi G\rho(R) \tag{4.12}$$

The potential will generally be axisymmetric, i.e., $\Phi = \Phi(R, z)$ (no dependence on angular coordinate ϕ).

In this case, use cylindrical coordinates and the components of Eq. (4.11):

$$\frac{d}{dt}\left(R^2\dot{\phi}\right) = 0 \tag{4.13}$$

$$\ddot{R} - R\dot{\phi}^2 = -\frac{\partial\Phi}{\partial R} \tag{4.14}$$

$$\ddot{z} = -\frac{\partial\Phi}{\partial z} \tag{4.15}$$

Rotation Curves, VII

Because $\frac{d}{dt}\left(R^2\dot{\phi}\right) = 0$:

The z-component of the angular momentum (per unit mass) is conserved:

$$L_z = R^2\dot{\phi} = \text{const.} \tag{4.16}$$

Introduce the effective potential

$$\Phi_{\text{eff}} = \Phi(R, z) + \frac{L_z^2}{2R^2} \tag{4.17}$$

to simplify Eq. (4.13)ff. further to obtain

$$\ddot{R} = -\frac{\partial\Phi_{\text{eff}}}{\partial R} \quad \text{and} \quad \ddot{z} = -\frac{\partial\Phi_{\text{eff}}}{\partial z} \tag{4.18}$$

Multiply by $\dot{R}$ and integrate to obtain the energy equation

$$\frac{1}{2}\dot{R}^2 + \Phi_{\text{eff}}(R, z) = \text{const.} \tag{4.19}$$

Rotation Curves, VIII

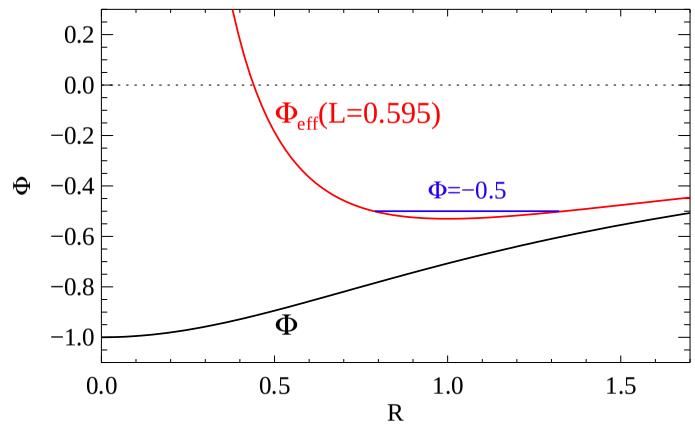

Energy equation defines the orbits of stars, yields (in general complicated) orbits between minimum and maximum radius.

Note "angular momentum barrier" for small R.

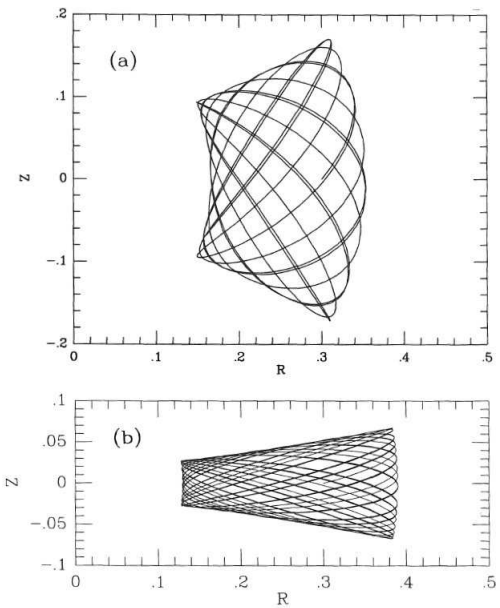

Figure 3-3. Two orbits in the potential of equation (3-50) with $q = 0.9$. Both orbits are at energy $E = -0.8$ and angular momentum $L_z = 0.2$, and we assume $v_0 = 1$.

Binney & Tremaine (Fig. 3.3)

Rotation Curves, X

To derive mass of galaxy from observed motion, a possible Ansatz is to assume circular orbits and to write

$$v^2(R) = R\frac{\partial\Phi}{\partial R} \tag{4.20}$$

where Φ is some suitable potential. An ansatz originally due to Alar Toomre is to notice that

$$\Phi_\pm(R,z) = \exp(-k|z|)J_0(kR) \tag{4.21}$$

is a solution of Laplace equation (J_0: Bessel function).

The surface density distribution causing this potential is (use Gauss' theorem; assume $z = 0$)

$$\Sigma_k(R) = -\frac{k}{2\pi G}J_0(kR) \tag{4.22}$$

Real surface densities can be generated by superposition:

$$\Sigma(R) = \int_0^\infty S(k)\Sigma_k(R)dk = -\frac{1}{2\pi G}\int_0^\infty S(k)J_0(kR)kdk \tag{4.23}$$

and the corresponding potential is

$$\Phi(R,z) = \int_0^\infty S(k)\Phi_k(R,z)dk = \int_0^\infty S(k)J_0(kR)e^{-k|z|}dk \tag{4.24}$$

Exponential Disks, I

It is possible to show that

$$S(k) = -2\pi G\int_0^\infty J_0(kR)\Sigma(R)RdR \tag{4.25}$$

Remember similar quantities for Fourier series!

$\Longrightarrow$ Obtain $\Sigma(R)$ from observations, then get $S(k)$

The predicted velocity profile is then:

$$v^2(R) = R\left.\frac{\partial\Phi}{\partial R}\right|_{z=0} = -R\int_0^\infty S(k)J_1(kR)kdk \tag{4.26}$$

For exponential disks, $\Sigma(R) = \Sigma_0\exp(-R/R_\mathrm{d})$, one finds

$$S(k) = -\frac{2\pi G\Sigma_0 R_\mathrm{d}^2}{[1+(kR_\mathrm{d})^2]^{3/2}} \tag{4.27}$$

and after a little bit tedious calculation

$$v^2(R) = 4\pi G\Sigma_0 R_\mathrm{d} y^2\left[I_0(y)K_0(y) - I_1(y)K_1(y)\right] \tag{4.28}$$

where I_j, K_j: modified Bessel functions and $y = R/(2R_\mathrm{d})$.

Exponential Disks, II

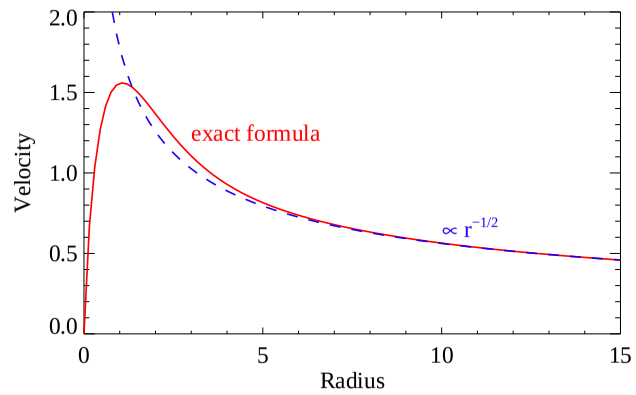

For a disk, the velocity is predicted to fall at sufficiently large radii, $v \propto r^{-1/2}$

As expected:

$$\frac{GM(\le r)}{r^2} = \frac{v_\mathrm{rot}^2(r)}{r} \quad\Longrightarrow\quad v = \sqrt{\frac{GM}{r}} \tag{4.29}$$

Exponential Disks, III

What mass distribution do we expect?

Intensity profile of disk in spiral galaxies can be well described by

$$I(r) = I_0\exp(-r/h) \tag{4.1}$$

Therefore the luminosity emitted within the radial distance r_0 is:

$$L(r<r_0) = I_0\int_0^{r_0}\exp(-r/h)\,2\pi r\,\mathrm{d}r = 2\pi I_0\left(h^2 - \exp(-r_0/h)h(h+r_0)\right) \tag{4.30}$$

i.e., for $r_0 \longrightarrow \infty$: $L(r<r_0) \to$ const..

$\Longrightarrow$ If all light comes from stars, i.e., light traces mass, and the population of stars does not change with position then $M/L \sim$ const..

This implies that outside of a certain radius $M(<r) \sim$ const. and thus $v \propto r^{-1/2}$

This is not what is observed!

Dark Matter Halos, I

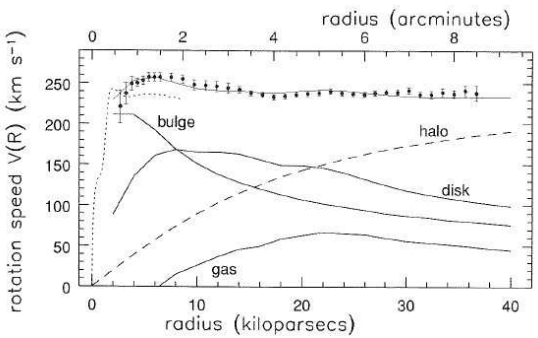

Radial Velocity Curve of NGC 7331 (SG, Fig. 5.20)

To obtain the flat rotation curves, disk profiles are not sufficient.

One therefore postulates a massive halo, e.g., with a density distribution of the form

$$\rho_{\rm halo}(R) = \frac{\rho_0}{1+(R/a)^\gamma} \quad \Longrightarrow \quad v^2_{\rm halo} = \frac{4\pi G}{r}\int_0^r x^2 \rho_{\rm halo}(x)\,dx \qquad (4.31)$$

Dark Matter Halos, II

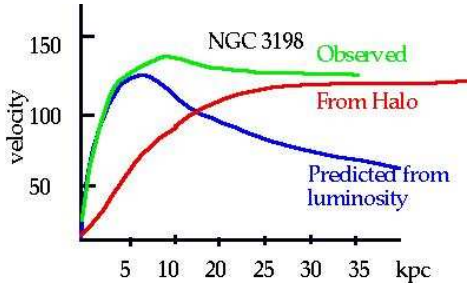

Distribution of dark matter:

- luminosity to mass ratio: $M/L = 4$ (solar neighbourhood)
- convert luminosity to mass
- compute expected rotation curve form the mass distribution $v_{\rm lum}(R)$
- distribution of dark matter:

$$M_{\rm dark}(R) = \frac{M}{G}\left[v^2(R) - v^2_{\rm lum}(R)\right] \qquad (4.32)$$

Canonical interpretation: a large fraction of gravitating material does not emit light $\Longrightarrow$ spiral galaxies have large and massive halos made of dark matter

In general, the mass to light ratio of spiral galaxies is $5 \lesssim M/L \lesssim 25$.

Tully-Fisher

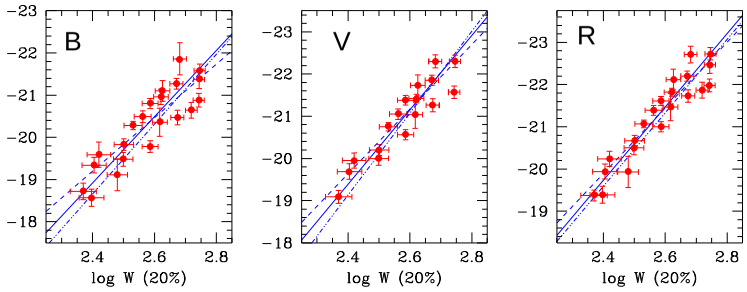

(after Sakai et al., 2000, Fig. 1)

The constant M/L for spirals leads to the Tully-Fisher relation for spiral galaxies: The width of 21 cm line of H is correlated with the galaxy luminosity, can be used as a distance indicator:

$$M = -a\log\left(\frac{W_{20}}{\sin i}\right) - b \qquad (4.33)$$

where W_{20}: 20% line width (km s^{-1}; typically $W_{20} \sim 300$ km s^{-1}), i inclination angle.

For the B- and I-Bands (Sakai et al., 2000):

	B	I
a	7.97± 0.72	9.24± 0.75
b	19.80± 0.11	21.12± 0.12

Tully-Fisher

Qualitative Physics: Line width related to mass of galaxy: $W/2 \sim V_{\rm max}$, where $V_{\rm max}$ max. velocity of rotation curve

$\Longrightarrow$ Assume $M/L =$ const. (good assumption)

$\Longrightarrow$ width related to luminosity.

The detailed physical basis is still unknown. Might be related to galaxy formation ("hierarchical clustering", see later).

I-band is better (less internal extinction).

Caveats:

1. Determination of inclination i.
2. Influence of turbulent motion within galaxy.
3. Constants dependent on galaxy type (Sa and Sb similar, Sc more luminous by factor of ∼2).
4. Optical extinction.
5. Intrinsic dispersion ∼0.2 mag.
6. Barred Galaxies problematic.

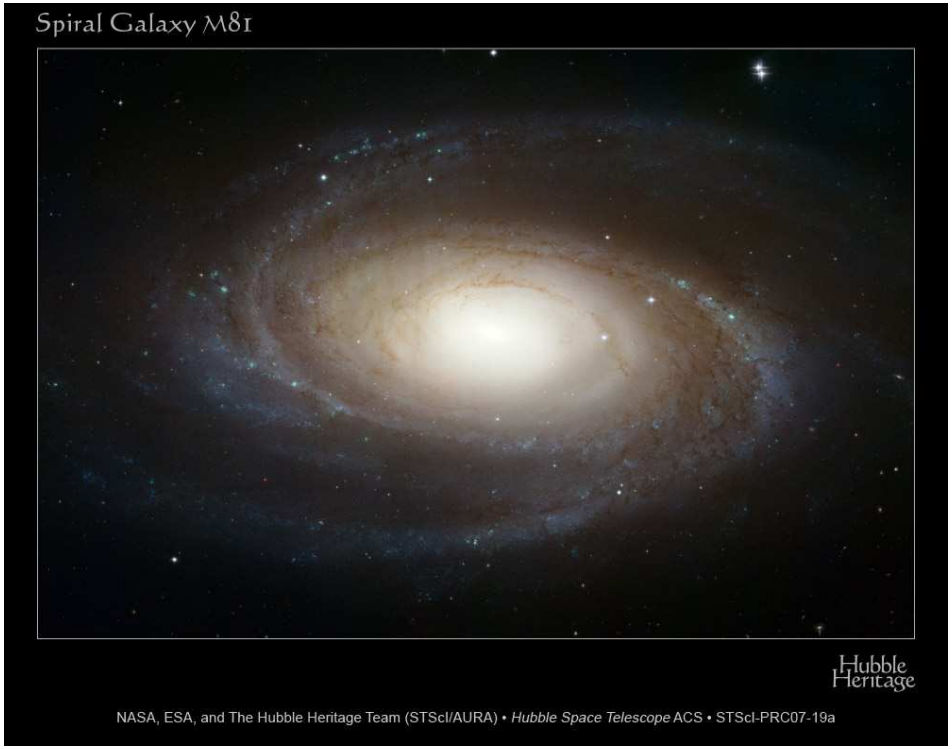

M100, “grand design spiral galaxy” (NOAO)

Spiral Patterns, III

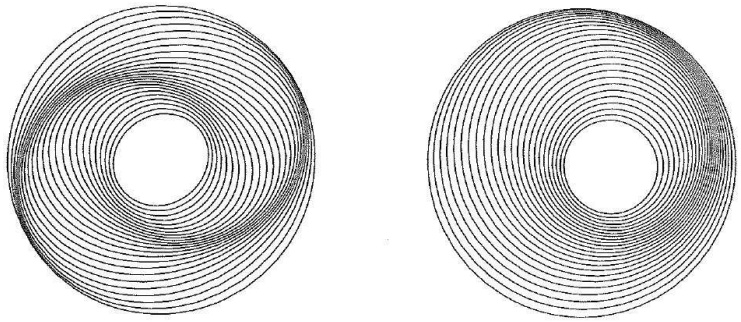

$R = R_g(1 + 0.075\cos(2(5 - 5R_g + \phi)))^{-1}$ and $R = R_g(1 + 0.15\cos((5 - 5R_g + \phi)))^{-1}$ (SG, Fig. 5.28)

Spiral arms can be generally described via

$$\cos\left(m\left(\phi + f(R,t)\right)\right) = 1 \tag{4.34}$$

where R, Φ: galactocentric coordinates, m: number of arms

$f(R,t)$ describes winding: $|\partial f/\partial R|$ large $\longrightarrow$ tightly wound arms.

Spiral Patterns, IV

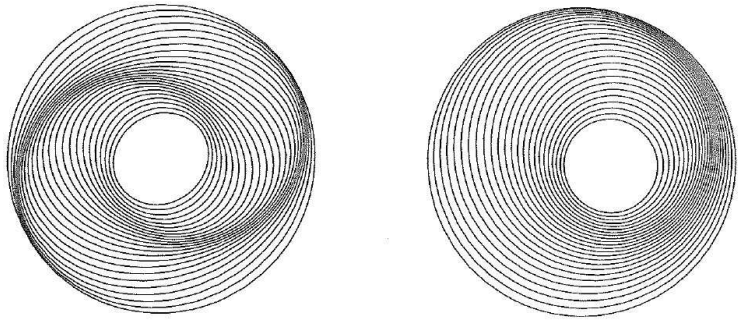

$R = R_g(1 + 0.075\cos(2(5 - 5R_g + \phi)))^{-1}$ and $R = R_g(1 + 0.15\cos((5 - 5R_g + \phi)))^{-1}$ (SG, Fig. 5.28)

Opening angle of spiral (“pitch angle”):

$$\cot i = \frac{1}{\tan i} = \left|R\frac{\partial\phi}{\partial R}\right| = \left|R\frac{\partial f}{\partial R}\right| \tag{4.35}$$

for Sa-galaxies: $i \sim 5°$, for Sc $10° < i < 30°$.

Constant pitch angles lead to logarithmic spirals, $f(R,t) = \ln R +$ const..

Winding Problem

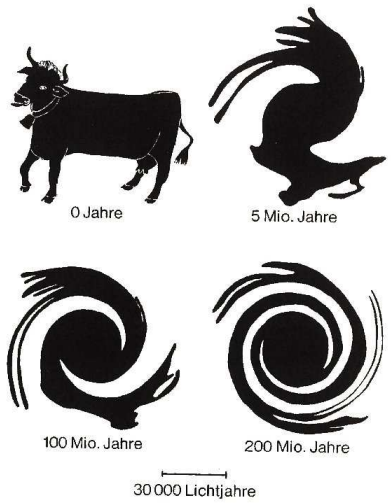

Winding Problem: differential rotation in the Galaxy would smear out any structures (=spiral arms) in a short time:

- Assume stars on straight line, i.e., $\phi = \phi_0$
- Stars move on circular orbits with $\Omega(R) = V(R)/R$, i.e. at time t: $\phi(t) = \phi_0 + \Omega(R)t$, i.e., $f(R,t) = -\phi_0 - \Omega(R)t$.
- Since $\Omega(R)$ drops: trailing spiral develops

Example for solar vicinity ($R = 8$ kpc, $V(R) \sim 200$ km s^{-1} and roughly constant):

$$\cot i = \frac{200}{8}\left(\frac{t}{1\,\text{Gyr}}\right) \Longleftrightarrow i \sim 2^\circ\left(\frac{t}{1\,\text{Gyr}}\right) \tag{4.36}$$

$\Longrightarrow$ very fast winding up

Kippenhahn

Epicyclic Orbits

To explain spiral pattern, we need to look at motions of stars in greater detail.

Of special interest: orbits around the minimum of the effective potential,

$$\nabla\Phi_{\text{eff}} = 0 \tag{4.37}$$

This means:

z-direction: gradient is 0 at $z = 0$

R-direction:

$$\frac{\partial\Phi_{\text{eff}}}{\partial R} = 0 \quad\Longrightarrow\quad \left.\frac{\partial\Phi}{\partial R}\right|_{R_g,z=0} = \frac{L_z^2}{R_g^3} = R_g\dot{\phi}^2 \tag{4.38}$$

$\Longrightarrow$ centrifugal force!

$\Longrightarrow$ circular orbit with angular speed $\dot{\phi}$!

The effective potential has a minimum at the radius of the circular orbit which has the angular momentum corresponding to L_z.

Epicyclic Orbits

Now look at small deviations in motion around $R = R_g$. Introduce

$$x = R - R_g \tag{4.39}$$

(which is a small quantity). In this case (Taylor!):

$$\Phi_{\text{eff}} \sim \frac{1}{2}\left(\kappa^2x^2 + \nu^2z^2\right) + \mathcal{O}(xz) + \ldots \tag{4.40}$$

where

$$\kappa^2 = \left.\frac{\partial^2\Phi_{\text{eff}}}{\partial R^2}\right|_{R_g,0} = \left.\frac{\partial^2\Phi}{\partial R^2}\right|_{(R_g,0)} + \frac{3L_z^2}{R_g^4} \quad\text{and}\quad \nu^2 = \left.\frac{\partial^2\Phi}{\partial z^2}\right|_{(R_g,0)} \tag{4.41}$$

But for circular motion

$$\left.\frac{\partial\Phi}{\partial R}\right|_{(R_g,0)} = \frac{L_z^2}{R_g^3} = R_g\Omega^2(R_g) \tag{4.42}$$

where Ω is angular speed of circular orbit at $R = R_g$, such that

$$\kappa^2 = \left(R\frac{d(\Omega^2)}{dR} + 4\Omega^2\right)_{R=R_g} \tag{4.43}$$

Epicyclic Orbits

Now insert Φ_{Eff} into equations of motion and solve them:

- z-direction:

$$\ddot{z} = -\frac{\partial\Phi_{\text{eff}}}{\partial z} = -\nu^2 z \quad\Longrightarrow\quad z(t) = Z\cos(\nu t + \zeta) \tag{4.44}$$

- x-direction:

$$\ddot{x} = -\kappa^2 x \quad\Longrightarrow\quad x(t) = X\cos(\kappa t + \psi) \tag{4.45}$$

- ϕ-direction:

$$\dot{\phi} = \frac{L_z}{R^2} = \frac{L_z}{R_g^2}\left(1 + \frac{x}{R_g}\right)^{-1} \sim \Omega_g\left(1 - \frac{2x}{R_g}\right)$$

$$\Longrightarrow\quad \phi(t) = \Omega_g t + \phi_0 - \frac{2\Omega_g X}{\kappa R_g}\sin(\kappa t + \psi) \tag{4.46}$$

The motion of stars close to the circular orbit can be described as a circular motion plus an elliptical motion around this guiding center.

Similar to pre-Keplerian theories of planetary motion $\Longrightarrow$ "epicyclic approximation"

Epicyclic Orbits

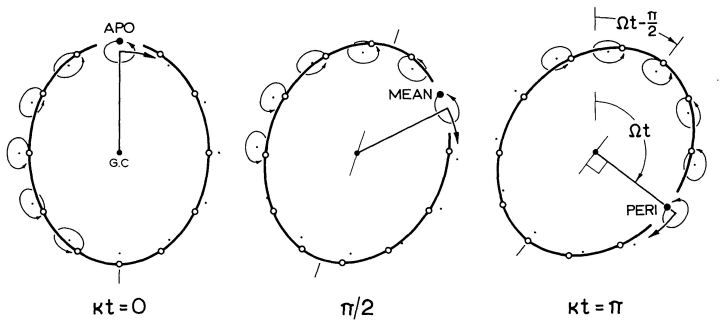

(Toomre, 1977, Fig. 2)

Epicyclic motion produces a spiral pattern (see figure, Sparke & Gallagher, and Toomre 1977), with pattern speed

$$\Omega_p = \Omega - \kappa/2 \tag{4.47}$$

Hubble Heritage Team, ESA, NASA

Spiral Arms

9

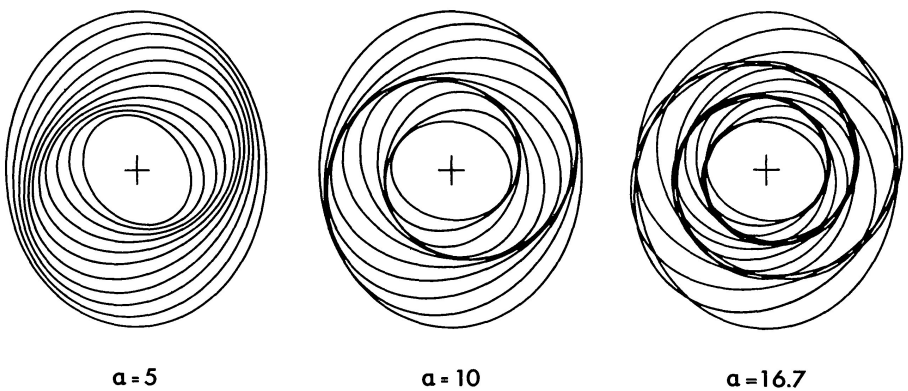

(Toomre, 1977, Fig. 3)

With this different types of spirals can be formed: Density wave theory

SSRO-South (R.Gilbert,D.Goldman,J.Harvey,D.Verschatse) - PROMPT (D.Reichart)

Observations

About half of all disk galaxies show a central linear bar!

Shape can be box-like or as extreme as 1 : 5 in ratio of short to long axis.

Edge-on view of disk galaxies tells us that bars are as thin as the disks themselves.

In contrast to spiral arms, bars occur in gas-rich and gas-poor systems.

Bars are not density waves!

It is not well understood why some galaxies are barred, while others are not.

Spiral arms usually start from the ends of bars

⇒ Bars are rotating with the same pattern speed as spiral arms.

Numerical Calculation

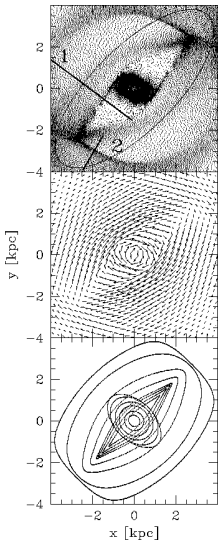

Numerical calculation of particle distribution and velocity field of test particles in bars possible.

Particle orbits close on themselves in corotating frame.

Velocity gradients along the orbits cause shocks

⇒ Gas and dust are compressed

⇒ Dust lanes along the bar major axis

⇒ Energy dissipation leads to angular momentum transport

⇒ Gas inflow toward galaxy center

Englmaier & Gerhard (1997)

Bulges, I

Bulges are among the densest stellar systems.

Surface brightness approximated by Sérsic's formula (empirical!):

$$I(R) = I(0)\exp\left[-(R/R_0)^{1/n}\right] \quad . \tag{4.48}$$

For $n = 1$, exponential decrease; for $n = 4$, de Vaucouleurs formula (developed for elliptical galaxies).

$$R \to 0\text{: } I \to \infty.$$

Observed values reach thousands of stars per cubic parsec.

Condon J.J., 1992, araa 30, 575

Englmaier P., Gerhard O., 1997, MNRAS 287, 57

Pagel B.E.J., 2009, Nucleosynthesis and Chemical Evolution of Galaxies, CUP, Cambridge, 2nd edition

Prantzos N., 2008, In: C. Charbonnel & J.-P. Zahn (ed.) Stellar Nucleosynthesis: 50 years after B2FH, Vol. 32. EAS Publ. Ser., p.311

Regan M.W., Thornley M.D., Bendo G.J., et al., 2004, ApJS 154, 204

Regan M.W., Thornley M.D., Vogel S.N., et al., 2006, ApJ 652, 1112

Rybicki G.B., Lightman A.P., 1979, Radiative Processes in Astrophysics, Wiley, New York

Sakai S., Mould J.R., Hughes S.M.G., et al., 2000, ApJ 529, 698

Seigar M., Carollo C.M., Stiavelli M., et al., 2002, AJ 123, 184

Shu F.H., 1991, The Physics of Astrophysics, Vol. I. Radiation, University Science Books, Mill Valley, CA

Toomre A., 1977, ARA&A 15, 437